Research Article | Vol. 28, No. 11 / 25 May 2020 / Optics Express 16244
Optics EXPRESS

Modeling Er/Yb fiber lasers at high powers

LIANG DONG,[1,*] TURGHUN MATNIYAZ,[1] MONICA T. KALICHEVSKY-DONG,[1] JOHAN NILSSON,[2] AND YOONCHAN JEONG[3]

[1]ECE/COMSET, Clemson University, 91 Technology Drive, Anderson, SC 29625, USA
[2]ORC, Southampton University, Southampton SO17 1BJ, UK
[3]ECE/ISRC/IAP/GSEP, Seoul National University, Seoul 06288, South Korea
[*]dong4@clemson.edu

Abstract: Conventional models of Er/Yb co-doped fibers assume all ytterbium ions are equally involved in the energy transfer with erbium ions, governed by a singular transfer rate. This would predict output power clamping once ytterbium parasitic lasing starts, contrary to the observations that the output continued to grow albeit at a slower rate. One study explained this using elevated temperature at high powers. Our study, however, shows that elevated temperature and mode-dependent effects only play insignificant roles. A new model is developed based on the existence of isolated ytterbium ions, which can explain all the observed experimental behaviors.

1. Introduction

Increasing demands for eye-safe LIDAR, sensing, and defense in recent years have attracted strong interest in further power scaling at ~1.56μm. For this, Er/Yb co-doped fibers are a leading platform. They were initially developed to allow Nd solid-state lasers to pump erbium-doped fiber amplifiers beyond the power levels available with single-mode diode pumps [1,2]. More recently, Er/Yb fibers have been used to power scale double-clad fiber lasers [3–8]. Double-clad fibers enable the use of high-power multimode diode pumps but require much higher pump absorption than that available from erbium ions in single-mode configurations with typical core and cladding diameters.

Er/Yb fiber amplifiers and lasers have been modeled by several authors [9–15]. All these models assume that all ytterbium ions are equally involved in the energy transfer process which is governed by a singular transfer rate. We show in this work that this model results in the prediction that, at high powers in a fiber laser, the pumping rate will eventually exceed the energy transfer rate, leading to an energy transfer bottleneck, resulting in increasingly higher ytterbium inversion. Ytterbium parasitic lasing will inevitably happen, leading to all erbium and ytterbium inversions being clamped at levels appropriate to compensate for the round-trip cavity losses for the respective ytterbium and erbium fiber lasers. The erbium output power is consequently clamped by the fixed energy transfer rate at the clamped inversion levels. This is, however, not what was observed in Er/Yb fiber lasers at high powers, where the output power continued to grow albeit at a slower rate [4,6,7,8].

One attempt has been made to explain this using the elevated fiber temperatures at high powers, which can increase re-absorption of ytterbium emission [13]. The increased re-absorption of ytterbium emissions means a higher ytterbium inversion at ytterbium lasing threshold, and therefore, a higher erbium output power. However, this current study has found that this re-absorption of ytterbium emission does not increase much with pump power and, consequently, the output from erbium ions would still be clamped in this case albeit at a slightly higher level.

One more possible explanation is from the observation that the M^2-value of the erbium emission was 3.9 while that of the ytterbium was 12 in [8]. It is easy to imagine that erbium is lasing in the lower-order modes while ytterbium is lasing in higher-order modes away from the

#393853 https://doi.org/10.1364/OE.393853
Journal © 2020 Received 27 Mar 2020; revised 17 Apr 2020; accepted 7 May 2020; published 13 May 2020

Optics EXPRESS

core center due to a combination of gain competition and higher V value at the ytterbium laser wavelength. This might lead to partial spatial separation of the erbium and ytterbium lasers. In a few-mode fiber, however, all modes have significant spatial overlap and our study still shows clamping of the output power from the erbium ions in this case.

To explain the observed behaviors in high-power Er/Yb fiber lasers, we have developed a new model in this work where some ytterbium ions are more isolated from energy transfer between erbium and ytterbium ions. This idea was first discussed in [8]. It is possible to imagine that some ytterbium ions are closely placed next to erbium ions and their related energy transfer can be modeled by a fast energy transfer rate. Considering the abundance of ytterbium ions relative to erbium ions, it is also easy to imagine that some ytterbium ions are isolated from erbium ions and in this case energy transfer to erbium ions would require emission of photons and eventual re-absorption by ytterbium ions placed next to erbium ions. Re-absorption directly by erbium ions is possible but at near-zero probability due to the narrow and weak erbium absorption at ~980nm. Direct energy transfer between neighboring ytterbium ions is, however, possible. With this model, the onset of ytterbium parasitic lasing is mostly due to the elevated inversion of the isolated ytterbium ions, while the high energy transfer rate of the ytterbium ions closely coupled to erbium ions ensures the continued growth of the output power from erbium ions long after the onset of ytterbium lasing.

We have also incorporated a temperature-dependent model based on thermally excited populations among Stark levels of ytterbium ions. This temperature-dependent model is anchored in measured temperature-dependent loss like those described in [16]. With this new model, we can successfully explain the observed behaviors of high-power Er/Yb fiber lasers and account for the insignificant roles that elevated temperature and mode-dependent gain play.

2. Er/Yb model with isolated ytterbium ions

The energy diagrams of ytterbium and erbium are shown in Fig. 1, together with their cross-sections. The stimulated transition rates are denoted as W, transfer rate as C and lifetime as τ. Two types ytterbium ions are assumed, the coupled ($n_6{}^c$, $n_5{}^c$) and uncoupled ($n_6{}^{nc}$, $n_5{}^{nc}$) to erbium ions, and f is the fraction of coupled ions ($f = 1$ is 100% coupled). The cross-sections and radiative lifetime are assumed to be the same for both types. We assume $n_4 \approx 0$ and $\tau_{43} \approx 0$ as in a typical case. The rate equations can be written below, noting that the two types of ytterbium ions are coupled through common stimulated emission rates W, which considers all pump, signal, ytterbium ASE and erbium ASE in both directions. More explicitly, emission from one type of ytterbium ions can be absorbed by another type of ytterbium ions. Total ytterbium ASE gain is determined by the overall ytterbium inversion consisting of both types of ions. In other words, both types of ytterbium ions contribute towards ASE equally.

$$\frac{\partial n_2}{\partial t} = W_{12}n_1 + \frac{n_3}{\tau_{32}} - \frac{n_2}{\tau_{21}} - W_{21}n_2 - 2C_{up}n_2^2 \tag{1}$$

$$\frac{\partial n_3}{\partial t} = W_{13}n_1 + C_{63}n_1n_6^c + C_{up}n_2^2 - W_{31}n_3 - \frac{n_3}{\tau_{32}} - C_{36}n_3n_5^c \tag{2}$$

$$\frac{\partial n_6^c}{\partial t} = W_{56}n_5^c + C_{36}n_3n_5^c - W_{65}n_6^c - \frac{n_6^c}{\tau_{65}} - C_{63}n_1n_6^c \tag{3}$$

$$\frac{\partial n_6^{nc}}{\partial t} = W_{56}n_5^{nc} - W_{65}n_6^{nc} - \frac{n_6^{nc}}{\tau_{65}} \tag{4}$$

$$n_1 + n_2 + n_3 = N_{Er} \tag{5}$$

$$n_5^c + n_6^c = fN_{Yb} \tag{6}$$

$$n_5^{nc} + n_6^{nc} = (1-f)N_{Yb} \tag{7}$$

Optics EXPRESS

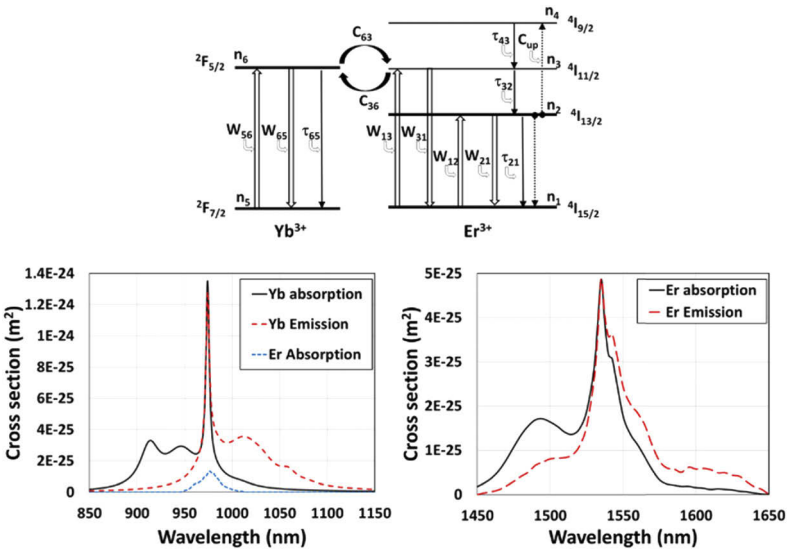

Fig. 1. Energy diagram of Er/Yb ions and relevant cross sections at T = 293 K.

Stimulated transition rates are evaluated in conventional ways and mode overlap with the core is calculated as described on page 341 of [17]. The steady-state equations can be obtained by setting the temporal derivatives to zero. The equations for solving the coupled erbium and ytterbium ions are not linear. By a process of elimination, a polynomial equation can, however, be found. We have further assumed that C_{63}=C_{36}, $W_{31}\approx 0$ as in all previous models.

$$\begin{aligned}
&\left(2W_{13}+W_{12}+\frac{1}{\tau_{32}}\right)C_{63}C_{up}n_2^3\\
&+\left[\begin{array}{l}\left(W_{21}W_{13}+\frac{W_{13}}{\tau_{21}}+\frac{W_{12}+W_{21}+W_{13}}{\tau_{32}}+\frac{1}{\tau_{21}\tau_{32}}\right)C_{63}-\\ \left(2W_{13}+W_{12}+\frac{1}{\tau_{32}}\right)\left(W_{56}+W_{65}+\frac{1}{\tau_{65}}+C_{63}N_{Er}\right)C_{up}-2\left(W_{56}+W_{65}+\frac{1}{\tau_{65}}\right)C_{63}C_{up}fN_{Yb}\end{array}\right]n_2^2\\
&+\left[\begin{array}{l}-\left(W_{21}W_{13}+\frac{W_{13}}{\tau_{21}}+\frac{W_{12}+W_{21}+W_{13}}{\tau_{32}}+\frac{1}{\tau_{21}\tau_{32}}\right)\left(W_{56}+W_{65}+\frac{1}{\tau_{65}}+C_{63}N_{Er}\right)\\ -\frac{W_{12}+W_{13}}{\tau_{32}}C_{63}N_{Er}-\left(W_{21}W_{56}+W_{12}W_{65}+W_{21}W_{65}+\frac{W_{56}+W_{65}}{\tau_{21}}+\frac{W_{56}}{\tau_{32}}+\frac{W_{12}+W_{21}}{\tau_{65}}+\frac{1}{\tau_{21}\tau_{65}}\right)C_{63}fN_{Yb}\end{array}\right]n_2\\
&+\frac{W_{12}+W_{13}}{\tau_{32}}N_{Er}\left(W_{56}+W_{65}+\frac{1}{\tau_{65}}+C_{63}N_{Er}\right)+\left(\frac{W_{56}}{\tau_{32}}+\frac{W_{12}}{\tau_{65}}+W_{65}W_{12}\right)C_{63}N_{Er}fN_{Yb}=0
\end{aligned}\tag{8}$$

The propagation equations are given below.

$$\frac{\partial I_P^{\pm}}{\partial Z}=\pm\{\Gamma_p[n_6\sigma_e^{Yb}-n_5\sigma_a^{Yb}-n_1\sigma_a^{Er}]-\alpha_p\}I_P^{\pm}\tag{9}$$

$$\frac{\partial I_s^{\pm}}{\partial Z}=\pm\{\Gamma_s[n_2\sigma_e^{Er}-n_1\sigma_a^{Er}]-\alpha_s\}I_s^{\pm}\tag{10}$$

$$\frac{\partial I_{YbASE}^{\pm}}{\partial Z}=\pm\{\Gamma_{YbASE}[n_6\sigma_e^{Yb}-n_5\sigma_a^{Yb}-n_1\sigma_a^{Er}]-\alpha_p\}I_{YbASE}^{\pm}\pm 2n_6\sigma_e^{Yb}\Delta f\tag{11}$$

$$\frac{\partial I_{ErASE}^{\pm}}{\partial Z}=\pm\{\Gamma_{ErASE}[n_2\sigma_e^{Er}-n_1\sigma_a^{Er}]-\alpha_s\}I_{ErASE}^{\pm}\pm 2n_2\sigma_e^{Er}\Delta f\tag{12}$$

where n_6=$n_6{}^{c}$+$n_6{}^{nc}$. I, Γ, σ, and N are respectively photon flux, mode overlap with active glass, cross section, and total dopant population. Subscript p, s, YbASE, ErASE a, and e indicate respectively pump, signal, Yb ASE, Er ASE, absorption and emission.

Optics EXPRESS

The thermal model is based on that given in [18,19]. The temperature distribution is quadratic in the core and logarithmic in the cladding. One thing to note is that the thermal transport from the core to the environment is largely limited by the heat transfer process at the fiber surface. The thermal conductivity of silica glass is relatively high and the temperature at the core is typically just a few degrees higher than that at glass surface, even for hundreds of microns of cladding [19]. We have assumed that the core temperature is uniform in our model, which is a reasonable approximation. The fiber temperature is largely determined by the heat transfer coefficient to the environment. Forced air cooling was used in [8], where the heat transfer coefficient is strongly dependent on both temperature and nature/velocity of the air flow at the fiber surface. These are not known in sufficient details. It is reasonable to believe that fiber temperature is well below 200°C as sustained exposure to higher temperature would lead to coating damage. The heat load along the fiber can, however, be easily calculated.

The model is implemented in Matlab. Pump, signal, ytterbium ASE and erbium ASE in both directions are considered. Photons are propagated forward and backward repeatedly using a standard ordinary differential equation solver (ode45) until convergence. Boundary conditions at each fiber end are set by the launched pump level and reflections (see Table 1). Guessed values are used as initial values for unknown powers. The process typically converges within 50 round-trip iterations to the required tolerance (typically <0.1% variation in powers from consecutive round-trip iterations in a consistent fashion).

Table 1. Nominal parameters used

Parameter	Value for [8]	Value for [4]	Notes
Core diameter	30μm	24μm	[8,4]
Cladding diameter	584μm	289.5μm	[8,4]
Core NA	0.21	0.2	[8,4]
τ_{21}	10ms	10ms	[14]
τ_{65}	1.3ms	1.3ms	[8,4]
τ_{32}	1ns	1ns	14]
C_{63}=C_{36}	2.98×10^{-20} m^3/s	2.15×10^{-20} m^3/s	Adjusted to fit data
C_{up}	3×10^{-24} m^3/s	3×10^{-24} m^3/s	[14]
N_{Er}	1.43×10^{25} ions/m^3	1.43×10^{25} ions/m^3	Erbium peak loss
N_{Yb}	2.45×10^{26} ions/m^3	1.12×10^{26} ions/m^3	Ytterbium peak loss
N_{Er}/ N_{Yb}	5.8%	12.8%	
Fraction of coupled Yb ions	15%	25%	Adjusted to fit data
Loss near 1.55μm	0.12dB/m	0.12dB/m	Estimated
Loss near 1μm	0.12dB/m	0.12dB/m	Estimated
Thermal conductivity	1.38 W/m/K	1.38 W/m/K	[17]
Fiber length	6m	5m	[8,4]
Reflection at pump end	4%	4%	[8,4]
Erbium reflection at far end	100%	100%	[8,4]
Ytterbium reflection at far end	5%	4%	[8,4]
Pump wavelength	975nm	975nm	[8,4]
Laser wavelength	1567nm	1565nm	[8,4]
Ytterbium ASE wavelength	1035-1075nm in 25 steps	1035-1075nm in 25 steps	
Erbium ASE wavelength	1540-1590nm in10 steps	1540-1590nm in10 steps	
Temperature	20°C uniform along fiber	20°C uniform along fiber	

Optics EXPRESS

The refractive index and dopant distributions are assumed to be uniform in the core. In our default case, all emission is in the fundamental mode. There is only a negligible amount of erbium ASE in all simulations and it is represented at 10 equally spaced wavelengths (5nm step size) while ytterbium ASE is represented at 25 equally spaced wavelengths (1.6nm step size). This is enough to resolve any spectral features. Ytterbium parasitic lasing can be clearly observed by a significant narrowing of the ytterbium ASE spectrum in the simulation as expected.

3. Modeling results

The nominal values of all parameters used in the model are given in Table 1 along with their sources and explanations. In cases where values used in the model deviated from these values in Table 1, the new values are specified where they occur. We first calculated the temperature-dependent ytterbium loss and small signal gain in the core for100% inversion of the fiber used in [8] as this is relevant to understanding the reabsorption of ytterbium ASE. This is given in Fig. 2. In general, loss at a wavelength shorter than 980nm decreases with a temperature rise since this absorption originates from the bottom level of the Stark split of $^2F_{7/2}$. The loss above 980nm increases with temperature as it originates from the upper levels of the Stark splits of $^2F_{7/2}$. The small signal gain decreases above ~1μm with a temperature rise due to a decrease of their excited state population at the bottom level of the Stark splits of $^2F_{5/2}$. At the peaks of gain and loss, these changes with temperature are more pronounced. Ytterbium parasitic lasing occurred at 1067nm in [8]. As shown in Fig. 2, the temperature dependence of the ytterbium gain and loss is very weak at this wavelength.

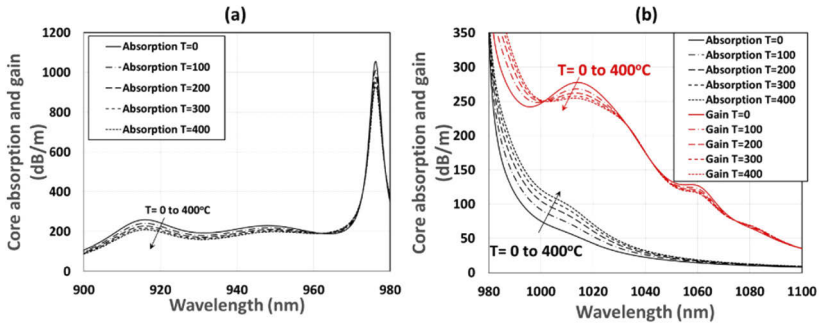

Fig. 2. Temperature dependence of (a) core absorption around the pump wavelength and (b) core absorption and small signal gain at 100% inversion around the ytterbium ASE wavelength from the model.

We first studied the case as in the conventional model where all ytterbium ions are equally involved in the energy transfer and described by a single transfer coefficient, i.e. the fraction of ytterbium ions coupled to erbium ions is 100% ($f = 1$). We studied two examples where the uniform temperature along the fiber length was set at 20°C and 500°C (far above what we considered realistic). The transfer coefficient C_{63} (=C_{36}) was adjusted to fit the measured Yb parasitic laser threshold in [8] at 20°C. The laser configuration was described in [8]. Briefly, the pump was launched into the fiber from free space. The cavity was formed at the pump end by straight cleaving and at the far end by butting with a dichroic mirror. The fiber was cooled by forced air. The results are shown in Fig. 3. It can be seen clearly that output powers are clamped to a fixed value in both cases, albeit that the output power is slightly higher for 500°C. This is because all the inversions are clamped to provide appropriate gains to compensate for the fixed respective cavity losses for the erbium and ytterbium lasers. This results in a fixed energy transfer rate (proportional to $C_{63}n_1n_6$) from ytterbium to erbium ions and consequently clamps the output power from the erbium ions. The conventional model even with the incorporation of

Optics EXPRESS

the temperature effect cannot explain the continued increase in output power from erbium after the onset of ytterbium parasitic lasing observed in [4,6,7,8]. In addition, the effect of temperature would be negligible for a temperature rise of just a few tens of degrees in a realistic scenario.

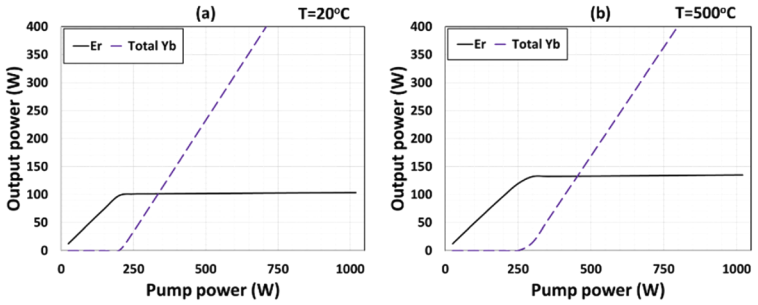

Fig. 3. Simulated powers from the Er/Yb fiber laser at two different temperatures predicted with the conventional model. All ytterbium ions are coupled to erbium ions ($f = 1$) and a uniform temperature along the fiber at (a) 20°C and (b) 500°C. C_{63}=C_{36}=1.1×10^{-21} m^3/s is determined by Yb threshold.

In addition, the authors in [13] used unrealistically high fiber temperature of 350°C to simulate the 103W Er/Yb fiber laser in [4]. This would lead to a fiber temperature of over 1000°C for the 297W Er/Yb fiber laser in [8]!

Another possible explanation of the observed continuous growth of Er/Yb fiber laser output after the onset of ytterbium parasitic lasing is that erbium is lasing in the lower-order modes while the ytterbium is lasing in higher-order modes away from the core center. This argument has its basis in the observed much higher M^2 values for the ytterbium parasitic laser than that of the erbium emission [8]. In a highly multimode fiber, this may happen due to ytterbium lasing in a combination of very high order modes (e.g. skew rays) with an overall doughnut pattern away from the core center. Lower-order modes, however, still have large overlap with such doughnut pattern, and their gain is still expected to be affected by such ytterbium lasing. In a few-moded fiber typically used in fiber lasers, even higher-order modes still have significant power near in the core center, leading to stronger gain competition with the lower-order modes.

There is a relatively large number of modes supported in the fiber in [8], making simulation very challenging when all the modes are considered. Given overall power of a combination of modes, finding power in each mode is impossible without knowing also the relevant phases. To gain some insight into how laser would behave when the erbium and ytterbium are lasing in separate patterns with some spatial separation, we simulated a simple case where the erbium laser is in the fundamental mode while the ytterbium laser is in a doughnut mode with the radial distribution of the LP_{11} mode. All the other parameters are the same as in Fig. 3(a). We divided the core into 10 uniform rings with equal thickness to be handled separately for this analysis. For the ytterbium and erbium ASE, the relevant modes are calculated at each ASE wavelengths. Within each ring, the inversions are calculated separately considering the local photon density of signal, pump, and ASE across all its wavelengths in both directions.

The results are shown in Fig. 4. Comparing Fig. 4(a) to Fig. 3(a), there is only a small difference. The laser output from erbium continues to grow after the onset of the parasitic lasing at ~200W of pump power. This growth is, however, very small, and the laser output is soon clamped to a level only slightly higher than that in Fig. 3(a). The radial distributions of inversions averaged longitudinally over the entire fiber length are shown in Fig. 4(b) for various pump powers. These pump powers are chosen to cover the range both below and above the ytterbium parasitic lasing threshold. The average erbium inversion is high near the core edge as expected. It shows very little change at various pump powers as the inversion is clamped

Optics EXPRESS

to provide an appropriate gain for the erbium laser. The average ytterbium inversion, on the other hand, increases with pump powers below ytterbium parasitic laser threshold and is largely clamped above the threshold. It is also high near the core edge due to the lower intensity of the doughnut pattern at this location. It shows some increase even above the threshold near the core center. This is due to the near-zero intensity of the doughnut mode near the core center. Such increase in inversion does not affect the gain much for the ytterbium parasitic laser.

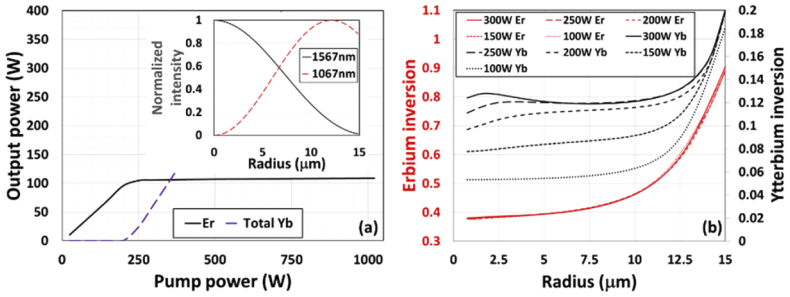

Fig. 4. Simulation signal output and total Yb output from the Er/Yb fiber laser with the conventional model. All ytterbium ions are coupled to erbium ions ($f = 1$) and erbium emission is in LP_{01} mode while ytterbium is in a doughnut pattern with LP_{11} radial distribution (intensities shown in the inset) (a) powers (b) average inversions across the core at various pump powers. C_{63}=C_{36}=1.1×10^{-21} m^3/s.

We finally studied the case where not all ytterbium ions are directly coupled to erbium ions ($f < 1$) with all powers in LP_{01} modes. The fraction of coupled ytterbium ions and the transfer coefficient C_{63} (=C_{36}) were first varied to get the best fit to the experimental data at the maximum power in [8] and the simulation was then run for the entire power range for $f = 0.15$, 0.2, 0.4, 0.6, 0.8 and 1 (Fig. 5(a)). Output clamping is clearly seen near $f = 1$, which needs to be lowered to get a best fit over the entire measured data range. The fraction of coupled ytterbium ions was determined to be 15% for the best fit. It is interesting to note that the ratio of erbium to ytterbium ions is ~5.8%, indicating, on average, one erbium ion being surrounded by roughly two and half neighboring ytterbium ions, if 15% of the ytterbium ions are coupled.

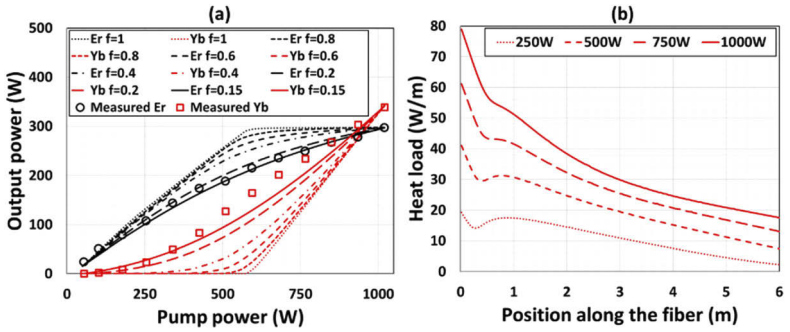

Fig. 5. (a) Simulated Er laser output and total Yb output by assuming 15%, 20%, 40%, 60%, 80% and 100% ytterbium ions being coupled to erbium ions ($f = 15\%$ with C_{63}=2.98×10^{-20} m^3/s, $f = 20\%$ with C_{63}=1.87×10^{-20} m^3/s, $f = 40\%$ with C_{63}=7.43×10^{-21} m^3/s, $f = 60\%$ with C_{63}=4.62×10^{-21} m^3/s, $f = 80\%$ with C_{63}=3.36×10^{-21} m^3/s, $f = 100\%$ with C_{63}=2.63×10^{-21} m^3/s) and (b) heat load at various pump powers for $f = 0.15$. Measured data is from [8].

Optics EXPRESS

As can be observed in Fig. 5(a), a reasonably good fit was achieved especially for the output power. There is some slight discrepancy in the fit to the total ytterbium parasitic laser output. We modeled ytterbium ions using only two types of ions, those closely coupled to erbium ions and those uncoupled to erbium ions. It may be more accurate to model the system based on a continuous change in the degree of the coupling. In addition, there is non-uniformity of dopants across the core in practice which is not considered here.

We have also simulated this case with ytterbium ASE in the doughnut mode with LP_{11} mode radial distribution. The results are very similar. Much higher-order modes might have been present in the ytterbium parasitic laser in [8] and this could also explain some of the discrepancy. Nevertheless, our current model seems to be enough to predict the generally observed behaviors. Figure 5(b) shows the heat load at various pump powers.

The inversions along the fiber for various pump powers and inversions averaged over the entire fibers versus pump powers are shown in Fig. 6. It can be seen in Fig. 6(b) that the average erbium inversion is clamped by the round-trip erbium cavity loss and so is the average inversion of the uncoupled ytterbium ions above ytterbium parasitic laser threshold by the round-trip ytterbium cavity loss. The average inversion of the coupled ytterbium ions, however, continues to increase with pump power, leading to a continued increase of ytterbium-to-erbium energy transfer and, consequently, to the increasing output power from erbium ions. This increase of average inversion of the coupled ytterbium ions also contributes slightly towards to the gain the ytterbium parasitic laser, leading to a slight decrease in the average inversion of the uncoupled ytterbium ions above the ytterbium laser threshold seen in Fig. 6(b).

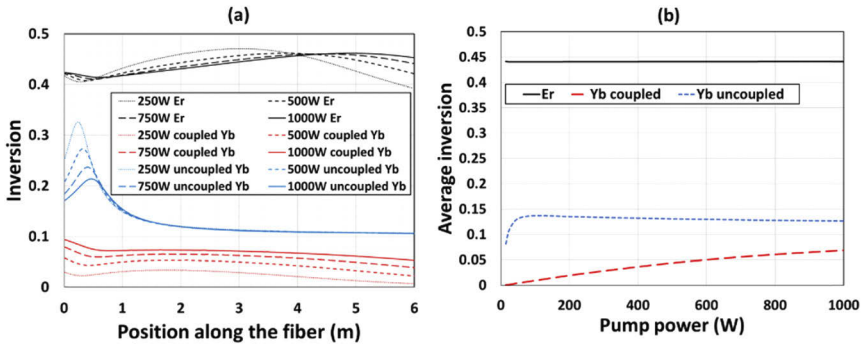

Fig. 6. (a) Inversion along the fiber and (b) average inversion over the entire active fiber for various pump powers for case of $f = 0.15$ in Fig. 5(a).

Strong re-absorption of ytterbium forward emission can be clearly seen by power decay during its propagation in our simulations (see Fig. 7(a)), previously also observed in [14]. This is true even at low pump power below ytterbium parasitic lasing threshold. Pump, signal and ASE powers inside the fiber are shown for 100W pump power in Fig. 7. Even in this case of 15% coupled ytterbium ions, pump is mostly absorbed. There are strong ASE inside the fiber but very little of it makes to the ends.

We have also modeled the results for the 103W Er/Yb fiber laser in [4] (see Fig. 8). The results are very similar. The fraction of coupled ytterbium ions was determined to be 25% in this case and the ratio of erbium to ytterbium ions is ~12.8%, indicating one erbium ion being on average surrounded by roughly two neighboring ytterbium ions.

Optics EXPRESS

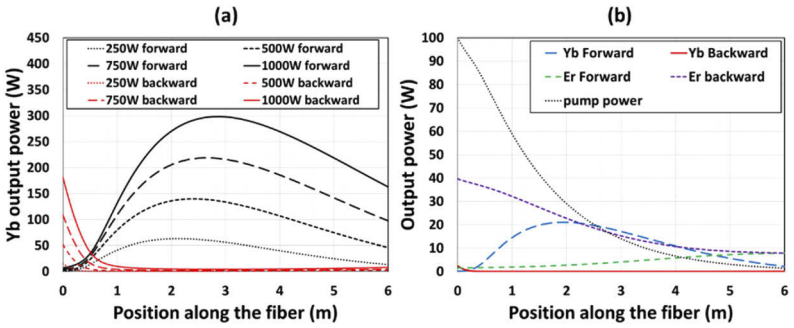

Fig. 7. (a) Ytterbium emission powers along the fiber at various pump powers for the model with $f = 0.15$ in Figs. 5(a) and (b) pump, signal, and Yb emission powers in the fiber at 100W of pump power.

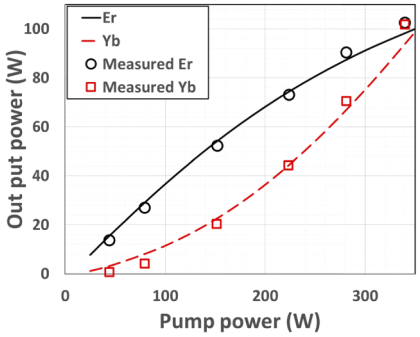

Fig. 8. Simulated Er output and total Yb output from the Er/Yb fiber laser for the experimental data in [4] ($f = 25\%$) (see Table 1 for details).

4. Discussion

In the light of the new insights, ytterbium parasitic lasing as a result of the bottleneck of energy transfer from ytterbium to erbium cannot be avoided. This will always take place at high enough pump powers when the pumping rate exceeds the energy transfer rate, i.e. $w_{56}n_5{}^c > C_{63}n_1n_6{}^c$. The energy transfer rate can be expressed as $C_{63}n_1n_6{}^c$, where C_{63} is determined by the host composition; n_1 is the erbium population at the ground state; and $n_6{}^c$ is the excited population of coupled ytterbium ions. For the case where all ytterbium ions are closely coupled to erbium ions, i.e. $f = 1$, the output power is expected to be clamped above the ytterbium parasitic lasing threshold by the fixed energy transfer rate which can now be written as $C_{63}n_1n_6$ where n_6 is the excited ytterbium population. This is because n_1 is fixed by erbium round-trip cavity loss and n_6 by ytterbium round-trip cavity loss. This is contrary to the experimental observation in [4,6,7,8].

Our work, for the first time, can explain this continuous output growth by resorting to two types of ytterbium ions, those closely coupled to erbium ions and those not closely coupled to erbium ions. In this case, when the above ytterbium parasitic lasing threshold, n_1 is still fixed, so is the population of the uncoupled ytterbium ions. The energy transfer rate $C_{63}n_1n_6{}^c$ can, however, still increase with pump power due to an increase in the population of the coupled ytterbium ions $n_6{}^c$, leading to a continuous increase in output power. Our model also reveals that there is significant re-absorption of the ytterbium ASE by the coupled ytterbium ions. This is very pronounced even at low pump powers, leading to significant radiative energy transfer from the uncoupled ytterbium ions to the coupled ytterbium ions and then some to erbium ions. This

Optics EXPRESS

explains the high laser efficiency observed at low pump powers in the simulation despite only a small fraction of ytterbium ions being closely coupled to erbium ions.

How can 40% slope efficiency possible if only 15% of ytterbium are coupled to erbium ions at low pump powers? The key to understand this is the significant amount of ASE generated in the fiber by the 85% uncoupled ytterbium ions which is then re-absorbed. For example, at pump power of 100W, i.e. below ytterbium parasitic laser threshold, ~98.5% of the pump is absorbed in the fiber. Co-propagating ASE reaches a level of ~21W mid-fiber, but it is mostly re-absorbed and only~2.2W ultimately leaves the fiber (see Fig. 7(b)). Backward ASE is also kept low by the re-absorption until the pumping end where the ytterbium inversion is relatively high.

The threshold pump power for the bottleneck of energy transfer can be written as $P_{th}= C_{63}n_1(n_6^c/n_5^c)Ahv_p/\sigma_a^{Yb}$, where A is pump core area; h is Planck's constant; v_p is the pump frequency; n_6^c/n_5^c is the inversion of the coupled ytterbium ions; and σ_a^{Yb} is the pump absorption cross section. This threshold of the ytterbium parasitic laser, however, can be increased by lowering pumping rate. One way is by pumping at ~915nm or ~940nm where the absorption cross section is much lower, i.e., lower σ_a^{Yb} . In fact, there are recent evidence for this [20,21]. Another way to lower pumping rate is by lowering the pumping intensity while maintaining the same pump power. This can be achieved by using a larger cladding, i.e., higher A. The threshold for ytterbium parasitic lasing can also be adversely affected by longer lifetime of the erbium $^4I_{11/2}$ level, which increases back energy transfer. High phosphorus doping can mitigate this by providing the high phonon energy required to increase the non-radiative decay of erbium $^4I_{11/2}$ level [22]. We have used very short lifetime of τ_{32}=1ns in our simulation to make it negligible as in [14]. Any increase in this life can severely lower the ytterbium parasitic lasing threshold.

A higher energy transfer rate will ease the bottleneck and raise the parasitic lasing threshold. To this end, a higher erbium doping level will be beneficial to increase n_1. Clearly it needs to be kept below the clustering levels.

A fluorescence decay measurement was conducted in [8] using a Q-switched laser at 920nm with 100ns pulse duration as the pump. The measurement showed significant decay (50% to 70%) within the first 10μs. This decay was believed to be caused by energy transfer from ytterbium to erbium. Roughly 2% of the ions relaxed with a time constant of 100μs or slower. The isolated ions were estimated to be 2-5% based on this. The energy transfer time can be calculated as $\tau_{63}=1/(C_{63}\times n_1)$. This gives τ_{63} a value of ~3μs based on our simulation when all erbium ions are in the ground state. Given the intensity of the Q-switched pump pulse of up to 30μJ, significant amount of ytterbium ions were inverted. If substantial energy transfer took place, erbium ions are expected to be nearly fully inverted after few hundreds of μs (noting τ_{63} depends on erbium ground state population and increases as erbium ions are inverted). This would have stopped any further energy transfer, leading to the decay to flat out after the initial energy transfer. This is then followed by a slower spontaneous decay.

Fluorescence decay measurements have been used in several works to evaluate energy transfer efficiencies in Er/Yb fibers [23–25]. Typically, the decay rate is used, and the magnitude of the intensity is rarely used. Low excitation is essential to avoid population saturation and ASE. The decay time of the fast decay component is typically in a range of 1-30μs followed by slow decay component with a decay time of 500μs to 1.3ms [24]. >50% of decay was observed during the fast decay for ytterbium concentrations exceeding 1.5wt% in [24]. These decays were not exponential especially when ytterbium concentration is high [23].

Non-radiative energy transfer among neighboring ytterbium ions can be very fast [23]. This likely also contributes towards the fast decay components when it leads to the excitation of erbium ions (or loss by other mechanisms) and may also explain the observed non-exponential decays. This additional effect will make the fast decay component far more pronounced than just direct ytterbium-to-erbium transfer. Although the decay rates of this additional energy transfer can be below 100μs, most of them are substantially slower than the few μs from the direct energy

Optics EXPRESS

transfer of ytterbium-to-erbium ions and consequently their contribution towards the easing of the bottleneck is less significant. Clearly more accurate modeling requires a better quantitative understanding of the non-radiative energy transfer process among the neighboring ytterbium ions. This is only possible with significant additional experimental studies.

In addition, there are also other processes which can contribute towards the fast decay component. An excited ytterbium ion can transfer energy to an erbium ion in the long-lived $^4I_{13/2}$ level leading it to be excited to $^4I_{9/2}$ [23] and up-conversion processes can also play a part. A quantitative modeling of the fluorescence decay process can be very helpful but is only possible with additional detailed experimental studies.

In any case, if 95% to 98% ytterbium ions are closely coupled to erbium ions derived by the proportion of fluorescence decay beyond 100μs in [8] and considering the ytterbium to erbium ratio of 1/0.058=~17 in this case, there will be 16 to 17 ytterbium ions on average being neighbors to a single erbium ion. This is not physically or chemically possible unless non-radiative neighboring ytterbium-ytterbium energy transfer is considered! There can only be a maximum of 4 ytterbium ions next to each erbium ion if rare earth ions are in the tetrahedral structure of silica. The fluorescence measurement in [8] would have included non-radiative energy transfer among neighboring ytterbium ions and significantly overstated the coupled ytterbium ions. Most of the decay processes involving energy transfer among neighboring ytterbium ions are significantly longer than the few μs decay time of the direct ytterbium-to-erbium energy transfer and consequently play a relatively much weaker role in the bottleneck process. There may also be other effects involved in the experiments. Further experimental studies are clearly needed.

Our work for the first time establishes a quantitative value for the energy transfer coefficient based on measurements in high-power lasers, $C_{63} = 2\text{-}3 \times 10^{-20}$ m^3/s. A decay time of $\tau_{63}=1/(C_{63}\times n_1) = 2\text{-}4\mu s$ can be derived for the fluorescence decay measurement. This is consistent with the fast end of the 1-30μs range measured in [24]. Our simulation also shows that only ~15% ytterbium ions are coupled to erbium ions in a fiber with erbium to ytterbium ratio of 0.058 and ~25% for a fiber with erbium to ytterbium ratio of 0.128. Based on these results, we can also show for the first time that on average there are 2-2.5 ytterbium ions next to a single erbium ion. From a material perspective, this is highly plausible in the tetrahedral structure of silica.

5. Conclusion

In conclusion, we have established a new Er/Yb model based on the existence of two types of ytterbium ions, those closely coupled to erbium ions and those uncoupled from erbium ions. We have incorporated an accurate temperature-dependent ytterbium cross section based on the measured temperature-dependent ytterbium loss. We have also studied the effect of ytterbium parasitic laser in a doughnut pattern while erbium in the fundamental mode. We concluded that the elevated temperatures at high powers and mode-dependent gain only play insignificant roles in the observed continuous growth of laser output from erbium after the onset of the ytterbium parasitic lasing. Based on the existence of two types of ytterbium ions, we can explain all the observed behavior in high-power Er/Yb fiber lasers in [4,6,7,8].

Funding

Army Research Office (W911NF-17-1-0454).

Disclosures

The authors declare no conflicts of interest.

Optics EXPRESS

References

1. M. E. Fermann, D. C. Hanna, D. P. Shepherd, P. J. Suni, and J. E. Townsend, "Efficient operation of an Yb-sensitized Er fiber laser at 1.56(m," Electron. Lett. **24**(18), 1135–1136 (1988).
2. S. G. Grubb, W. H. Hunter, R. S. Cannon, S. W. Vendetta, K. L. Sweeney, P. A. Leilabady, M. R. Keur, J. G. Kwasegroch, T. C. Munks, and D. W. Anthon, "24.6dBm output power Er/Yb codoped optical amplifier pumped by a diode-pumped Nd: YLF laser," Electron. Lett. **28**(13), 1275–1276 (1992).
3. P. K. Cheo and G. G. King, "Clad-pumped Yb:Er codoped fiber lasers," IEEE Photonics Technol. Lett. **13**(3), 188–190 (2001).
4. J. K. Sahu, Y. Jeong, D. J. Richarson, and J. Nilsson, "A 103W erbium-ytterbium co-doped large-core fiber laser," Opt. Commun. **227**(1-3), 159–163 (2003).
5. J. Nilsson, S. Alam, J. A. Alvarez-Chavez, P. W. Turner, W. A. Clarkson, and A. B. Grudinin, "High-power and tunable operation of erbium-ytterbium co-doped cladding-pumped fiber lasers," IEEE J. Quantum Electron. **39**(8), 987–994 (2003).
6. Y. Jeong, J. K. Sahu, D. B. S. Soh, C. A. Codemard, and J. Nilsson, "High-power tunable single-frequency single-mode erbium:ytterbium codoped large-core master-oscillator power amplifier source," Opt. Lett. **30**(22), 2997–2999 (2005).
7. D. Y. Shen, J. K. Sahu, and W. A. Clarkson, "Highly efficient Er/Yb doped fiber laser with 188W free-running and >100W tunable output power," Opt. Express **13**(13), 4916–4921 (2005).
8. Y. Jeong, S. Yoo, C. A. Codemard, J. Nilsson, J. K. Sahu, D. N. Payne, R. R. Horley, P. W. Turner, L. Hickey, A. Harker, M. Lovelady, and A. Piper, "Erbium:Ytterbium codoped large-core fiber laser with 297W continuous-wave output power," IEEE J. Sel. Top. Quantum Electron. **13**(3), 573–579 (2007).
9. J. Nilsson, P. Scheer, and B. Jaskorzynska, "modeling and optimization of short Yb^{3+}-sensitized Er^{3+}-doped fiber amplifiers," IEEE Photonics Technol. Lett. **6**(3), 383–385 (1994).
10. M. Karásek, "Optimum design of Er^{3+}-Yb^{3+} codoped fibers for large-signal high-pump power applications," IEEE J. Quantum Electron. **33**(10), 1699–1705 (1997).
11. G. C. Valley, "Modeling cladding-pumped Er/Yb fiber amplifiers," Opt. Fiber Technol. **7**(1), 21–44 (2001).
12. E. Yahel and A. A. Hardy, "Modeling and optimization of short Er^{3+}-Yb^{3+} codoped fiber lasers," IEEE J. Quantum Electron. **39**(11), 1444–1451 (2003).
13. G. Canat, J. C. Mollier, Y. Jaoulën, and B. Dussardier, "Evidence of thermal effects in high-power Er^{3+}-Yb^{3+} fiber laser," Opt. Lett. **30**(22), 3030–3032 (2005).
14. Q. Han, J. Ning, and Z. Sheng, "Numerical investigation of the ASE and power scaling of cladding-pumped Er-Yb codoped fiber amplifiers," IEEE J. Quantum Electron. **46**(11), 1535–1541 (2010).
15. X. Zhao, Q. Han, D. Wang, H. Hu, K. Ren, J. Jian, and T. Liu, "Optical design of high-power sacaded co-pumping Er/Yb-codoped fiber lasers," Opt. Lett. **44**(5), 1100–1103 (2019).
16. X. Peng and L. Dong, "Temperature dependence of ytterbium-doped fiber amplifiers," J. Opt. Soc. Am. B **25**(1), 126–130 (2008).
17. A. W. Snyder and J. D. Love, *Optical Waveguide Theory*, (Chapman and hall, 1983).
18. M. K. Davis, M. J. F. Digonnet, and R. H. Pantell, "Thermal effects in doped fibers," J. Lightwave Technol. **16**(6), 1013–1023 (1998).
19. D. C. Brown and H. J. Hoffman, "thermal, stress, thermal-optic effects in high average power double-clad silica fiber lasers," IEEE J. Quantum Electron. **37**(2), 207–217 (2001).
20. D. Creeden, H. Pretorius, J. Limongelli, and S. D. Setzler, "Single frequency 1560 nm Er:Yb fiber amplifier with 207W output power and 50.5% slope efficiency," Proc. SPIE **9728**, 97282L (2016).
21. O. D. Varona, W. Fittkau, P. Booker, T. Theeg, M. Steinke, D. Kracht, J. Neumann, and P. Wessels, "Single-frequency fiber amplifier at 1.5(m with 100W in the linearly-polarized TEM00 mode for next-generation gravitational wave detectors," Opt. Express **25**(21), 24880–24892 (2017).
22. J. E. Townsend, W. L. Barnes, K. P. Jedrzejewski, and S. G. Grubb, "Yb^{3+} sensitised Er^{3+} doped silica optical fibre with ultrahigh transfer efficiency and gain," Electron. Lett. **27**(21), 1958–1959 (1991).
23. M. Laroche, S. Girard, J. K. Sahu, W. A. Clarkson, and J. Nilsson, "Accurate efficiency evaluation of energy-transfer processes in phosphosilicate Er^{3+}–Yb^{3+}-codoped fibers," J. Opt. Soc. Am. B **23**(2), 195–202 (2006).
24. M. A. Melkumov, A. Y. Laptev, M. V. Yashkov, N. N. Vechkanov, A. N. Guryanov, and I. A. Bufetov, "Effects of Yb^{3+} and Er^{3+} Concentrations and Doping Procedure on Excitation Transfer Efficiency in Er–Yb Doped Phosphosilicate Fibers," Inorg. Mater. **46**(3), 299–303 (2010).
25. M. M. Khudyakov, A. S. Lobanov, D. S. Lipatov, A. N. Abramov, N. N. Vechkanov, A. N. Guryanov, M. A. Melkumov, K. K. Bobkov, S. S. Aleshkina, T. A. Kochergina, L. D. Iskhakova, F. O. Milovich, M. M. Bubnov, and M. E. Likhachev, "Single-mode large-mode-area Er–Yb fibers with core based on phosphorosilicate glass highly doped with fluorine," Laser Phys. Lett. **16**(2), 025105 (2019).